Archives of Acoustics Vol. 49, No. 4, pp. 601–612 (2024), doi: 10.24425/aoa.2024.148806

Research Paper

A Study of Acoustic Emission Based RA-AF Characteristics of Polypropylene Fiber-Reinforced Recycled Aggregate Concrete Under Uniaxial Compression

Daowen ZHOU[(1),(2)], Xin YANG[(1),(2),(4)*], Yu TANG[(1),(2)], Yutao MIAO[(3)]

[(1)] *School of Civil Engineering, Fujian University of Technology*
Fuzhou, China

[(2)] *Key Laboratory of Underground Engineering, Fujian University of Technology*
Fuzhou, China

[(3)] *Chengtong Branch, China Railway Second Group Co., Ltd.*
Chengdu, China

[(4)] *School of Civil Engineering, Fuzhou University*
Fuzhou, China

*Corresponding Author e-mail: yangxin546@163.com

(*received November 30, 2023; accepted April 10, 2024; published online August 6, 2024*)

In order to research the acoustic emission characteristics of polypropylene fiber-reinforced recycled aggregate concrete under uniaxial load, 20 groups of test specimens with a coarse aggregate substitution rate of 25 % and 50 % are designed and fabricated to conduct the acoustic emission test under uniaxial compression, and the evolution laws of the acoustic emission *b*-value, the cracking modes and the acoustic emission RA-AF moving averages with time are studied. The laws of influence of the coarse aggregate substitution rate and coarse-fine polypropylene fiber on the acoustic emission *b*-value of RAC are discussed. The *K*-means clustering method is adopted for two-dimensional clustering analysis of the shear cracking and tensile cracking, and then the SVM is used to obtain the boundary between the two types of clusters. The time distribution laws of shear cracking and tensile cracking of the polypropylene fiber-reinforced recycled aggregate concrete are analyzed. The changes in the moving averages of RA and AF of RAC test specimens with time are studied, and the research indicates that as the RA value decreases, the shear cracking gradually reduces and the tensile cracking gradually increases and dominates.

Keywords: polypropylene fiber-reinforced recycled aggregate concrete; acoustic emission characteristics; *b*-value; RA-AF; moving average.

1. Introduction

The current topic is how to improve the performance of recycled aggregate concrete (RAC). There are mainly two optimization schemes: first, when making recycled aggregate, the cement mortar on the surface is treated with chemical reagents to make the internal voids in aggregate smaller, thus increasing the RAC performance; second, fiber materials are added to improve the tensile and compressive strength and toughness of RAC. Steel fibers have been widely used and popularized due to their very evident anti-crack effect since their application to concrete. However, steel fibers also have some shortcomings. When steel fibers were applied in a humid and corrosive environment, the service life of concrete would be significantly reduced due to its susceptibility to corrosion. Polypropylene fiber is a type of reinforced and toughened material, with good corrosion resistance, light weight, easy dispersion, little damage to mixing machines, low price, and other advantages, which better overcomes the shortcomings of steel fiber.

In recent years, many scholars have studied the acoustic emission characteristics of RAC, including RAC modification (adding silica fume – Bai *et al.*, 2022), replacement of coarse and fine aggregates (copper slag as fine aggregate – Prem *et al.*, 2018), replacement of coarse and fine aggregates with plastic wastes (Belmokaddem *et al.*, 2020), recycled sand as fine aggregate (Fardoun *et al.*, 2022), and crumb rubber as fine aggregate (Assaggaf *et al.*, 2022), and aggregate proportion (Guo *et al.*, 2017). Watanabe *et al.* (2007) tested the microcracks in concrete under compression applying the acoustic emission technique. Kencanawati *et al.* (2013) introduced an acoustic emission parameter analysis model for analyzing the concrete cracking behavior.

The acoustic emission (AE) technique can be used to study damage evolution and identify failure modes (Aki, 1965; Utsu, 1965; Lockner *et al.*, 1991; Unander, 1993; Weiss, 1997; Greenhough, Main, 2008; Kwiatek *et al.*, 2014; Liu *et al.*, 2020a; 2020b; Chen *et al.*, 2022). In addition, many achievements had been made in the research of acoustic emission characteristics of fiber-reinforced concrete, including compression performance (Menna *et al.*, 2022), bending test (Adamczak-Bugno *et al.*, 2022a; 2022b; Mandal *et al.*, 2022), shear behavior (Goyal *et al.*, 2022), uniaxial tension (De Smedt *et al.*, 2022), and cyclic load (Xargay *et al.*, 2021). Goyal *et al.* (2021) established the empirical relationship between the damage index and the acoustic emission parameter by the genetic algorithm. Essassi *et al.* (2021) classified the acoustic emission signals by the K-means algorithm and found three different classes of cracking events: fiber cracking, matrix cracking, and fiber debonding. Lauff *et al.* (2021) added short fibers to fresh concrete and processed the material with a 3D printer to orient the fibers, thus obtaining a material with high uniaxial strength properties. Jung *et al.* (2021) proposed a new parameter, namely, the composite b-value, to analyze the distribution of the acoustic emission amplitude at the crack origin. Prem *et al.* (2021) reported that acoustic emission parameters were closely related to different failure mechanisms (shear, shear flexure, and flexure).

To sum up, the polypropylene fiber-reinforced RAC test was conducted under uniaxial compression in this work to obtain the acoustic emission information in the fracturing process and analyze the evolution law of the AE based b-value and the AE based RA-AF (RA is defined as the ratio of rise time to amplitude; AF is defined as the ratio of counts to duration). Based on K-means clustering and support vector machine, the cracking modes of polypropylene fiber-reinforced recycled aggregate concrete were studied. On this basis, a whole-process analysis was made based on the time history of the acoustic emission characteristic, which was of great theoretical and practical significance.

2. Experimental details

2.1. Specimen preparation

The polypropylene fiber used for the test is produced by Hebei Xinqixiang Polypropylene Fiber Technology Co., Ltd., with its physical and mechanical parameters shown in Table 1.

The cement used is ordinary Portland cement of grade 42.5, the fine aggregate is medium sand in zone II with a particle size of 0.15 mm–4.75 mm and the natural coarse aggregate is the gravel with a particle size of 5 mm–20 mm, among which the 5 mm–10 mm and 10 mm–20 mm aggregates are in a 2:3 ratio. The recycled coarse aggregates are produced with waste concrete with a base material strength grade of C30 by way of mechanical crushing and screening, as shown in Fig. 1.

Table 1. Physical and mechanical indicators of polypropylene fiber.

Fiber no.	Diameter [mm]	Length [mm]	Tensile strength [MPa]	Fracture strength [MPa]	Elongation at break [%]	Initial modulus [GPa]	Density [g/cm^3]	Recommended dosage [kg/m^3]
FF1	0.036	12	≥ 300	360	30	3.5	0.91	0.9
FF2	0.036	19	≥ 450	450	17	4.8	0.91	0.9
CF1	0.9	30	≥ 550	500	24	6.6	0.91	6.0
CF2	0.9	50	≥ 550	500	24	6.6	0.91	6.0

Fig. 1. Coarse and fine aggregates of RAC: a) fine aggregates; b) natural coarse aggregates; c) recycled coarse aggregates.

Table 2. Test plan for C30 polypropylene fiber-reinforced RAC.

Specimen no.	Mixing amount of coarse aggregate [kg/m^3]		Coarse aggregate substitution rate [%]	Fiber length [mm]	Fiber dosage [kg/m^3]
	Natural	Recycled			
R-25-0	840.63	280.21	25	None	0
R-25-1	840.63	280.21		12	0.9
R-25-2	840.63	280.21		19	0.9
R-25-3	840.63	280.21		30	6
R-25-4	840.63	280.21		50	6
R-25-5	840.63	280.21		12 + 30	0.9 + 5.1
R-25-6	840.63	280.21		12 + 50	0.9 + 5.1
R-25-7	840.63	280.21		19 + 30	0.9 + 5.1
R-25-8	840.63	280.21		19 + 50	0.9 + 5.1
R-25-9	840.63	280.21		12 + 19 + 50	0.45 + 0.45 + 5.1
R-50-0	560.42	560.42	50	None	0
R-50-1	560.42	560.42		12	0.9
R-50-2	560.42	560.42		19	0.9
R-50-3	560.42	560.42		30	6
R-50-4	560.42	560.42		50	6
R-50-5	560.42	560.42		12 + 30	0.9 + 5.1
R-50-6	560.42	560.42		12 + 50	0.9 + 5.1
R-50-7	560.42	560.42		19 + 30	0.9 + 5.1
R-50-8	560.42	560.42		19 + 50	0.9 + 5.1
R-50-9	560.42	560.42		12 + 19 + 50	0.45 + 0.45 + 5.1

In this test, the concrete with a strength grade of C30 is used, and the number of test groups is 20, with 3 test specimens for each group. It is calculated that the mix proportion of C30 polypropylene fiber-reinforced RAC is: cement 358 kg/m^3, medium sand 706.15 kg/m^3, coarse aggregate 1,120.85 kg/m^3, and water 215 kg/m^3. Each group of concrete uses the same mix proportion, and only the coarse aggregate substitution rate and fiber dosage are different. Among them, the recycled coarse aggregate substitution rate for R-25 and R-50 is 25 % and 50 %, respectively. As a reference test specimen, R-25-0 should be made of plain concrete, without adding any fiber to it. R-25-1, R-25-2, R-25-3, and R-25-4 are four test specimens, each mixed with a different kind of polypropylene fiber. The fiber dosage is 0.9 kg/m^3 for R-25-1 and R-25-2 test specimens into which one kind of fine polypropylene fiber is added, respectively, and 6.0 kg/m^3 for R-25-3 and R-25-4 into which one kind of coarse fiber is added, respectively, according to the instruction manual of the polypropylene fiber manufacturer. R-25-5, R-25-6, R-25-7, R-25-8, and R-25-9 are the test specimens into which both fine and coarse fibers are added. To ensure the test comparability, the total dosage of coarse and fine fibers is controlled to 6.0 kg/m^3 as shown in Table 2.

2.2. Experimental setup

With reference to the related provisions in (GB/T 50081-2019, 2019), a 150 mm × 150 mm × 150 mm standard test cube is designed for the test. After being molded, all the test specimens are left at room temperature for 1D, numbered for removal of their forms, and cured in the standard curing room for 28 days before the cube compression test is carried out. The machine used for the cube compression test of polypropylene fiber-reinforced RAC is the HCT306B microcomputer-controlled electro-hydraulic servo press, and the test specimen is loaded at a speed of 0.5 MPa/s until the test specimen is ruptured.

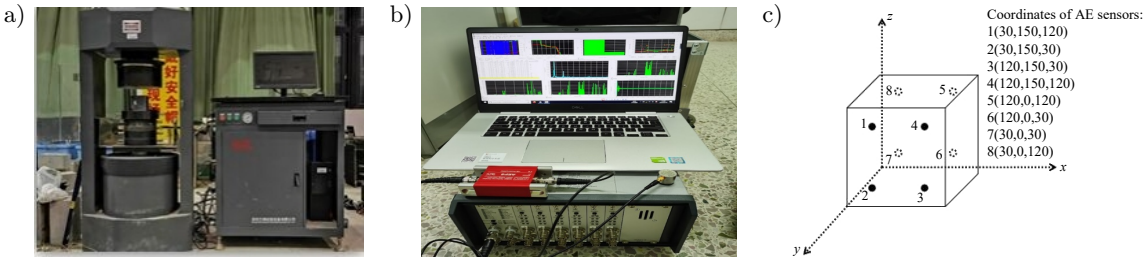

Fig. 2. Test apparatus: a) HCT306B press; b) AMSY-6 acoustic emission instrument; c) acoustics emission sensor arrangement (applied load acts parallel to the z-axis on the plane above the specimen).

The acoustic emission acquisition system is an AMSY-6 acoustic emission instrument. During the test, 8 acoustic emission sensors are fixed on the surface of polypropylene fiber-reinforced RAC (this work selects the channel with the third highest number of acoustic emission events for analysis). To ensure that the acoustic emission sensor and RAC can be fully coupled, a layer of vacuum adhesive is applied to the contact position between the acoustic emission sensor and RAC. To eliminate the effect of environmental noise upon the test, the threshold value and the sampling frequency of the acoustic emission instrument are set as 40 dB and 5 MHz, respectively.

2.3. Characteristics of AE based b-value

Gutenberg and Richter (1944) proposed the famous expression of statistical relation between earthquake magnitude and frequency:

$$\log_{10} N = a - bM, \tag{1}$$

where M is the magnitude, N is the earthquake frequency of magnitude in ΔM, a and b are constants, and the b-value is a function of the relative magnitude distribution. In this work, the b-value is calculated by replacing the magnitude M with the acoustic emission amplitude, therefore the b-value is a function of the crack growth scale, whose dynamic change characteristics are of direct physical significance. The least square method is adopted in this work to calculate the b-value. A hundred pieces of acoustic emission amplitude data are taken as the sampling window each time, the sliding window is 50, and the magnitude interval ΔM is set to 0.2 dB. In the data processing process, the occurrence of the last acoustic emission amplitude from a hundred piece sampling window is regarded as the scale of the b-value.

Figure 3 illustrates the temporal variation of the AE based b-value of the RAC with a coarse aggregate substitution rate of 25 % and 50 % (the first specimen from each group was selected for the acoustic emission analysis in this work). The law of influence of the coarse aggregate substitution rate on the b-value is analyzed based on Fig. 3a. For no. 0 specimens not mixed with polypropylene fibers, the AE based b-value of R-25-0 specimen shows a continuous sharp decline in the initial phase, indicating a continuous increase of major event cracking; later, the b-value fluctuates up and down in a small range until the post-peak phase, indicating the stable growth of microcracks. The b-value of R-50-0 test specimen begins to increase slightly after 20 seconds, indicating an increase of minor event cracking; later, the b-value fluctuates in a small range; when the specimen is on the verge of failure, the b-value begins to decrease significantly until the post-peak phase, indicating a continuous increase of the major event cracking of the specimen.

It can be seen from the analysis of the changes of the AE based b-value in Fig. 3a that:

1) For both R-25-0 and R-50-0 RAC into which no polypropylene fibers are added, the b-value exhibits a continuous sharp decrease for R-50-0, indicating that a specimen (R-25-0) with a small content of recycled aggregate is probably more resistant to microcracking processes than R-50-0.
2) The b-value of R-50-0 test specimen decreases significantly in the post-peak phase, indicating a continuous increase of major event cracking in the post-peak phase. The b-value of R-25-0 shows a small increase in the post-peak phase. Therefore, on the whole, the post-peak strength of R-25-0 test specimen with a coarse aggregate substitution rate of 25 % is better than that of R-50-0 test specimen with a coarse aggregate substitution rate of 50 %.
3) The initial b-value of R-50-0 test specimen is smaller than that of R-25-0 test specimen probably because the more initial defects of R-50-0 test specimen lead to more major event cracking in the initial phase, making the initial b-value bigger.

From the analysis of the law of influence of adding one kind of fine polypropylene fiber on the b-value in Fig. 3b–c, it can be observed that, for R-25-1, R-25-2, R-50-1, and R-50-2 test specimens into which only one kind of fine fiber is added, respectively, their b-value do not decrease sharply until they are close to failing in the pre-peak phase, and that their b-value mainly increase slightly and slowly or fluctuate up and down in a small range. This indicates that with the addition of polypropylene fine fibers, the major event cracking is inhibited and the minor vent cracking dominates. When the test specimens are about to fail, the b-value decrease significantly, indicating that major event cracking increases gradually.

From the analysis of the law of influence of adding one kind of coarse polypropylene fiber on the b-value in Fig. 3b–c, it can be observed that, for R-25-3, R-50-3, R-25-4, and R-50-4 test specimens into which only one kind of coarse polypropylene fiber is added (fiber diameter: 0.9 mm; fiber length: 30 mm and 50 mm), their b-values are generally stable and begin to decrease significantly only when they are about to fail.

From the analysis of the law of influence of adding more than one kind of coarse polypropylene fiber on the b-value in Fig. 3f–j, it can be observed that, for R-25-6, R-50-6, and R-50-7 test specimens into which both coarse and fine fibers are added, their b-values are generally stable and begin to decrease significantly only when they are about to fail. The b-value of other test specimens into which more than one kind of fiber is added are characterized by ups and downs, demonstrating the intense evolution of microcracks.

a) No. 0 specimens without polypropylene fiber (mean value of *b*-value is 0.9155 and 0.884 for R-25-0 and R-50-0).

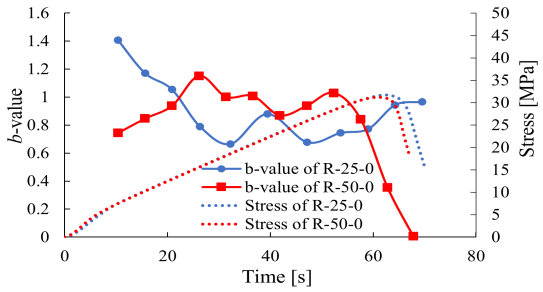

b) No. 1 specimens with fine fiber added (mean value of *b*-value is 0.9061 and 0.8655 for R-25-1 and R-50-1).

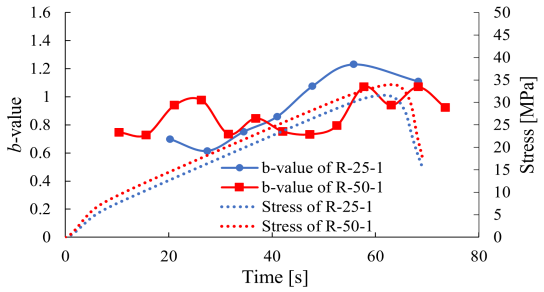

c) No. 2 specimens with fine fiber added (mean value of *b*-value is 0.7651 and 0.77 for R-25-2 and R-50-2).

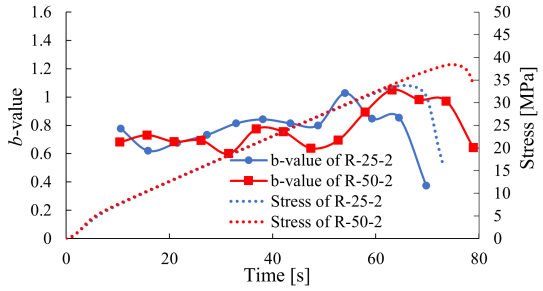

d) No. 3 specimens with coarse fiber added (mean value of *b*-value is 0.849 and 0.8457 for R-25-3 and R-50-3).

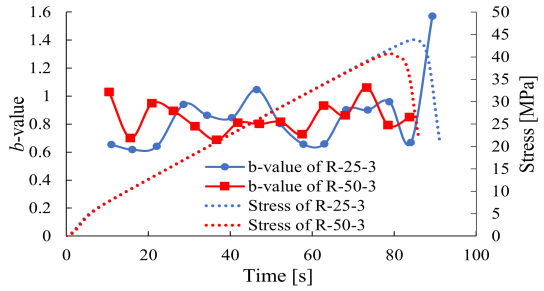

e) No. 4 specimens with coarse fiber added (mean value of *b*-value is 0.9252 and 1.005 for R-25-4 and R-50-4).

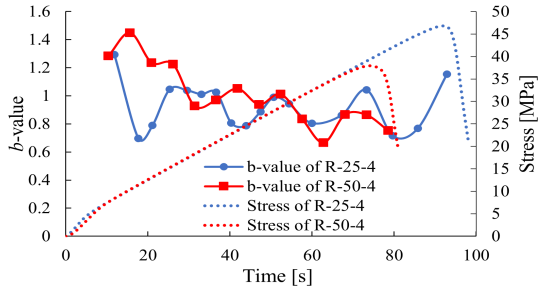

f) No. 5 specimens with coarse and fine fibers (mean value of *b*-value is 0.8757 and 0.8353 for R-25-5 and R-50-5).

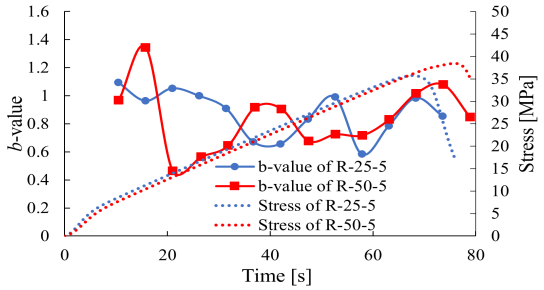

g) No. 6 specimens with coarse and fine fibers (mean value of *b*-value is 0.8144 and 0.7036 for R-25-6 and R-50-6).

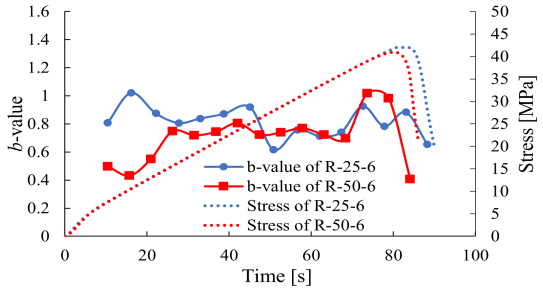

h) No. 7 specimens with coarse and fine fibers (mean value of *b*-value is 0.9027 and 0.8031 for R-25-7 and R-50-7).

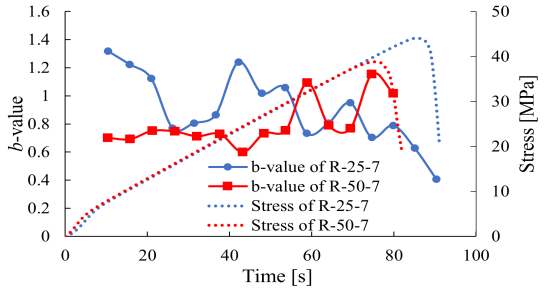

i) No. 8 specimens with coarse and fine fibers (mean value of *b*-value is 0.8392 and 0.8883 for R-25-8 and R-50-8).

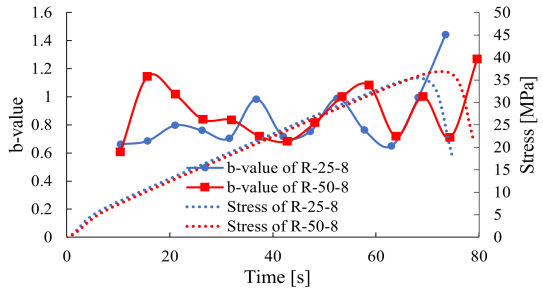

j) No. 9 specimens with coarse and fine fibers (mean value of *b*-value is 0.852 and 0.7833 for R-25-9 and R-50-9).

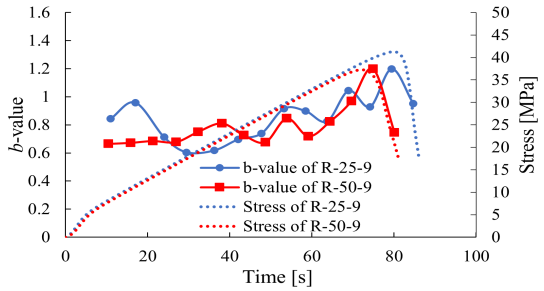

Fig. 3. Temporal variation of AE based *b*-value of RAC.

3. Analysis of polypropylene fiber-reinforced concrete cracking modes based on RA-AF method

Concrete cracking modes include tensile and shear modes of cracking. The correlation between RA and AF in acoustic emission parameters is related to the cracking modes of concrete materials and can be used to effectively identify the cracking modes of concrete materials.

Generally speaking, RA and AF values are different in terms of shear damage and tensile damage. In a tensile damage mode, the related AF value will be higher due to the release of energy. On the contrary, due to the long rise time and duration, the RA value related to the shear damage mode will be higher (Zhang, 2020). The RA and AF calculation principles are indicated in Eqs. (2) and (3), respectively:

$$\mathrm{RA} = \frac{\text{Rise time}}{\text{Amplitude}}, \tag{2}$$

$$\mathrm{AF} = \frac{\text{Counts}}{\text{Duration}}, \tag{3}$$

where rise time is the time interval during which the acoustic emission signal is raised to its maximum amplitude through a threshold, whose unit is μs; amplitude is the highest amplitude value of the acoustic emission waveform signal, whose unit is mV; counts is the number of times the single acoustic emission signal exceeds the threshold value, whose unit is dimensionless; duration is the time from the first time the acoustic emission signal exceeds the threshold value to the last time it drops to the threshold value, whose unit is μs.

Determining the RA-AF boundary is important to the differentiation between material cracking modes. The boundary is generally a straight line defined artificially. The acoustic emission event distributed to the upper left of the straight line is considered tensile cracking, while that distributed to the lower right of the straight line is considered shear cracking, as shown in Fig. 4. However, such a method can be easily affected by such factors as the sensor model and characteristic parameter selection. Consequently, an unsupervised machine learning technique – K-means clustering method is introduced in this work to differentiate between RA and AF.

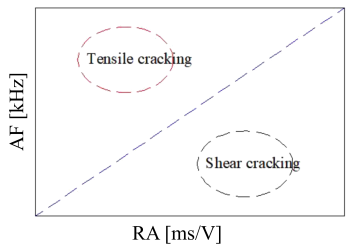

Fig. 4. Classification of typical cracking modes based on RA-AF relationship.

3.1. K-means clustering

K-means is a method of continuous iterative clustering. Its operating principle is: assuming that the sample data is n variables X_1 to X_n, these n variables are divided into k categories, and m_i is the mean value of these variables (MacQueen, 1967). The distance formula adopts the Euclidean distance, and the specific steps are as follows:

1) randomly and uniformly select K observation samples as the initial cluster center m_1 to m_k;
2) separate each sample data from its nearest cluster center;
3) update the mean vector of the cluster center according to the cluster center to which each sample belongs;
4) repeat steps 2 and 3. When the set number of iterations is reached or the mean vector of the cluster center is no longer updated, the model is built and the clustering algorithm results are derived.

3.2. Theory of support vector machines

The support vector machines (SVM) can find a suitable interface for the two types of data, so that the two types of data can be separated most completely. The interface is defined as the optimal hyperplane (Vapnik, 1999). Forming a new vector $\mathbf{y}$ ($\mathbf{y} = (X, L)$) with data X and its label L can form an n-dimensional vector space ($\mathbf{Y} = (y_1, ..., y_j, ..., y_n)$) for n data. In the vector space $\mathbf{Y}$, the hyperplane can be described by the following equation:

$$\omega^T X + d = 0, \tag{4}$$

where $\boldsymbol{\omega} = (\omega_1, \omega_2, ..., \omega_f)$ is the hyperplane normal vector, which is used to describe the direction of the hyperplane; d is the hyperplane displacement term, which is used to describe the distance of the hyperplane from the origin.

The vectors closest to the hyperplane in the two types of vectors are called support vectors, and the sum of the distances between two heterogeneous support vectors and the hyperplane is:

$$\gamma = \frac{2}{\|\omega\|}. \tag{5}$$

Find the optimal hyperplane, that is, calculate ω and d to make t the maximum value. If linear inseparability is considered, the objective function to be solved is shown in Eq. (5). At this time, some points are allowed not to meet the constraint condition (6):

$$f = \min_{\omega,d} \frac{1}{2} \|\omega\|^2 + C \sum_{i=1}^{m} L_{0/1} \left(y_i \left(\omega^T X_i + d \right) - 1 \right), \quad (6)$$

$$y_i \left(\omega^T X_i + d \right) \geq 1, \qquad i = 1, 2, ..., n, \quad (7)$$

where $L_{0/1}$ is 0–1 loss function, C is a constant greater than 0. When C is taken as a valid value, some data are allowed not to meet the constraint conditions. When C is taken as infinity, all data will be forced to meet the conditions.

3.3. Cracking modes analysis

In this work, the K-means clustering method is used for the two-dimensional clustering analysis of RA-AF values, so as to differentiate between shear and tensile cracking. Then, the recognition and classification function of the SVM is used to obtain the boundary between the two types of clusters, i.e., shear cracking and tensile cracking. In order to make the data meet the constraint conditions as much as possible, the constant C in Eq. (6) is set to 1.000 in this work. See Figs. 5–6 (note: the boundary of the compaction phase is determined by the stress-strain curve, which is the turning point of the stress-strain curve from an upward concave shape to an approximate straight line) and Table 3 for the calculation results. As can be seen from Fig. 5, the two types of cracking can be well differentiated by applying the K-means clustering method; the shear cracking is characterized by a high RA value, while the tensile cracking is characterized by a low RA value; the slopes of the linear RA-AF value boundaries of the two types of cracking obtained by the SVM are both close to 0. Most of the cracking of the polypropylene fiber-reinforced RAC is tensile cracking. As can be observed from Fig. 6 and Table 3, shear cracking is mainly distributed in the elastic-plastic phase and some test specimens have a few shear cracking in the compaction phase and the post-peak phase; there are a lot of tensile cracking in the three phases. In addition, in the latter half of the elastic-plastic phase, the RA value of the shear cracking reduces gradually; the shear cracking disappears within 5 s–18 s before the test specimen fails, and only tensile cracking exists in this time range. To sum up, the tensile cracking is in the majority in terms of the number of cracking modes. From the perspective of time distribution of cracking,

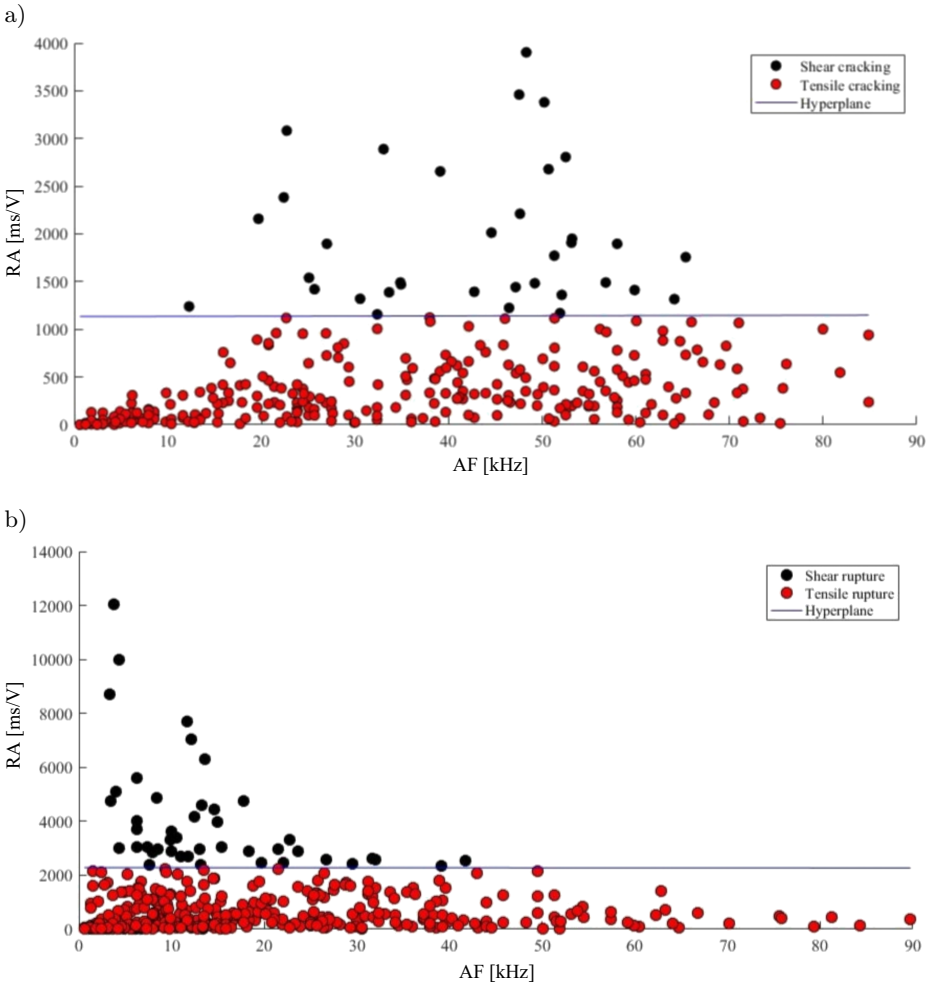

Fig. 5. Hyperplane calculation results of shear and tensile cracking: a) R-25-0; b) R-25-2.

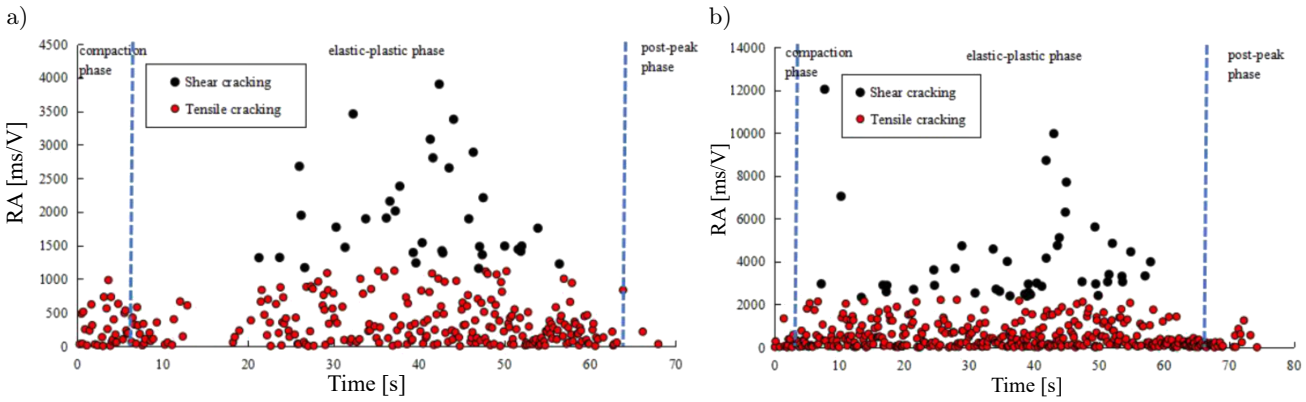

Fig. 6. Time distribution of shear and tensile cracking:
a) R-25-0; b) R-25-2.

Table 3. RA-AF value boundaries corresponding to different cracking modes of polypropylene fiber-reinforced RAC and shear cracking time distribution.

Specimen no.	Shear cracking and tensile cracking dividing line for RA-AF value RA = k^*AF + e		Time distribution of shear cracking [s]	Failure time of specimens [s]
	k [ms/V/kHz]	e [ms/V]		
R-25-0	0.1579	1134.5	21.3–56.4	62
R-25-1	0.0677	1433.8	2.2–52.5	62
R-25-2	–0.1487	2278.9	7.2–57.8	66
R-25-3	0.0885	1808.8	3.5–75	85
R-25-4	0.3166	2436.6	2.3–73.7	92
R-25-5	–0.368	1599.6	10.6–60.7	68
R-25-6	–0.0299	1918.2	2.4–72.9	81
R-25-7	0.1508	1679.8	14.6–78.8	86
R-25-8	–0.2016	1278.4	0.6–56.4	68
R-25-9	0.0592	2411.2	7.3–66	80
R-50-0	–0.4341	894.2	9.6–56.1, 63.1	61
R-50-1	0.8742	1375.4	3.2–49.4	63
R-50-2	0.6816	1284.7	7.9–65	75
R-50-3	–0.4768	1431.8	6.3–65.4	79
R-50-4	0.4683	677.0	3–66.6, 76.3	74
R-50-5	–0.3026	1170.5	8.5–68.1	76
R-50-6	0.0171	1522.7	2.8–65.3	80
R-50-7	0.1057	2084.3	5.3–66.9	75
R-50-8	0.0342	1941.9	7.6–60.7	73
R-50-9	0.3992	1553.7	3.4–59.7	72

the shear cracking is mainly concentrated in the first half of the elastic-plastic phase, and the tensile cracking is in the majority within 5 s–18 s before the test specimen fails. Therefore, the cracking mechanism of the polypropylene fiber-reinforced RAC under uniaxial compression is dominated by tensile cracking.

4. Whole-process analysis under uniaxial compression based on time history of acoustic emission characteristic parameters

As can be known from Eqs. (2) and (3) and the research results of Sec. 3, the RA value increases/decreases mainly depending on the increase/decrease of the shear cracking, while the AF value increases/decreases mainly depending on the intensity of acoustic emission activities. Figure 7 illustrates the changes in RA and AF moving averages of RAC test specimens with time. In order to reduce scattering and clearly reveal the trend, each point on the curve is the moving average of the last 100 acoustic emission data points and the time of the last data point of every 100 acoustic emission data points is taken as the scales of RA and AF.

Research findings:

1) As can be seen from Fig. 7, the RA moving averages of most test specimens exhibit an overall upward trend in the first half phase and an overall downward

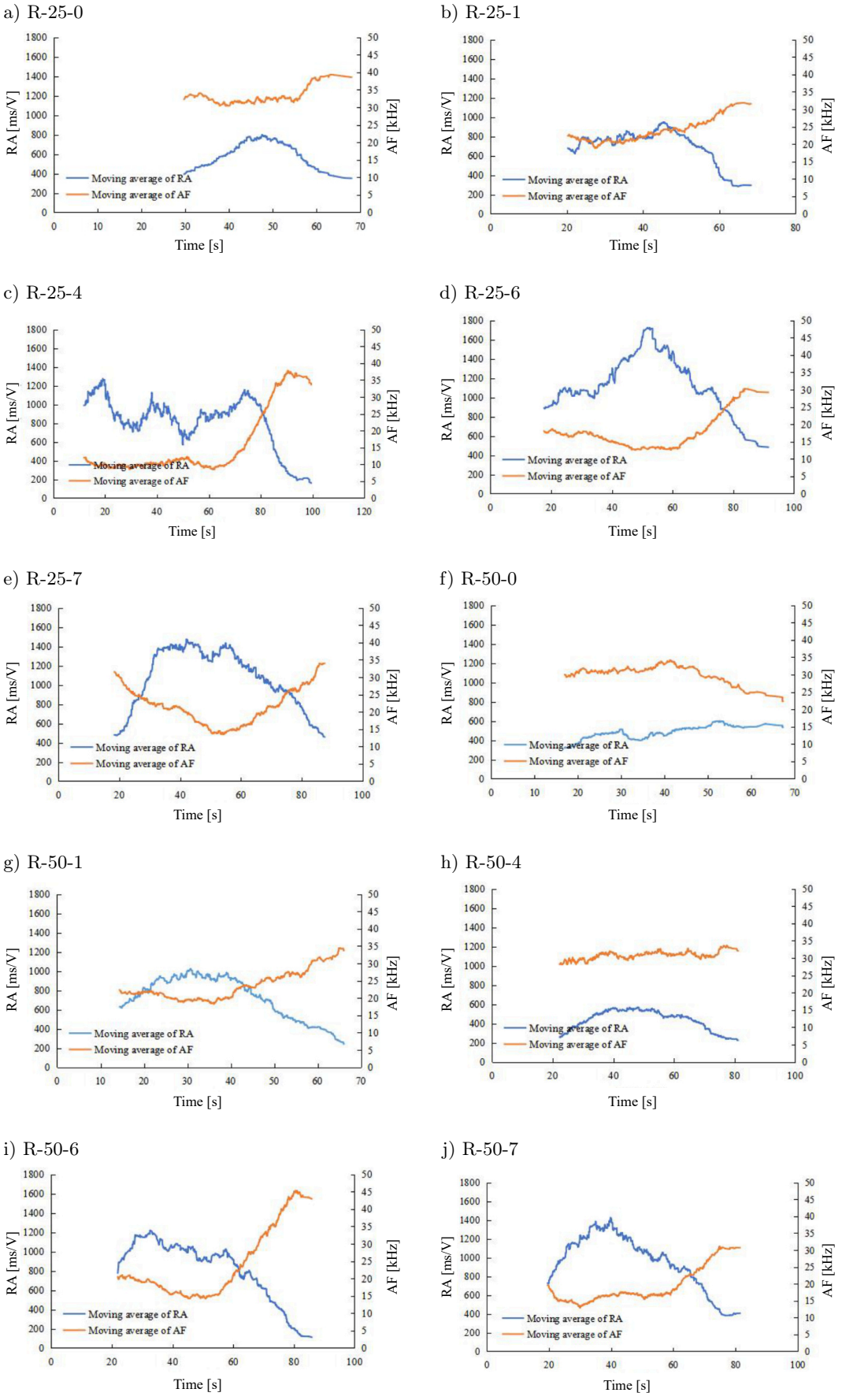

Fig. 7. Moving averages of acoustic emission RA and AF of RAC.

trend in the latter half phase. As the RA value decreases, the shear cracking gradually reduces and the tensile cracking gradually increases and dominates.

2) As can be observed from Fig. 7 and Table 4, the minimum values of the AF moving averages of most test specimens are negatively correlated with the RAC strength, namely the lower the minimum value of the AF moving average is, the higher the RAC strength will be. Among the RAC with a coarse aggregate substitution rate of 25 %, the minimum value of the AF moving average is 30.44 for R-25-0 test specimen into which no fiber is added and in the 8.53–18.87 range for the RAC into which coarse and fine fibers are added. Among the RAC with a coarse aggregate substitution rate of 50 %, the minimum value of the AF moving average is 22.31 for R-50-0 test specimen into which no fiber is added and is in the 12.91–28.13 range for the RAC into which coarse and fine fibers are added; Therefore, the minimum value of the AF moving average can be used to evaluate the reinforcement effect of polypropylene fibers on RAC. In concrete with a coarse aggregate substitution rate of 25 %, the minimum value of the AF moving average of R-25-4 test specimen is the minimum, showing the best reinforcement effect. In concrete with a coarse aggregate substitution rate of 50 %, the minimum values of the AF moving averages of R-50-6 and R-50-7 test specimens are the minimum, showing better reinforcement effects than other specimens.

3) There is a certain correlation between the AF value and the AE based *b*-value. When the AF value increases continuously, the corresponding *b*-value also increases continuously, indicating an increase in minor event cracking, as shown in Fig. 8a, R-25-1 test specimen in the 20 s–55 s range. When the AF value decreases continuously, there are two scenarios. One is that AF has a high initial value (more than 25 kHz) and decreases continuously. In this scenario, the AE based *b*-value also decreases continuously, indicating an increase in major event cracking, as shown in Fig. 8b,

Table 4. Relationship between minimum value of acoustic emission AF moving average and peak strength.

Specimen no.	Minimum values of the AF moving averages [kHz]	Peak stress [MPa]
R-25-0	30.44	31.384
R-25-1	18.87	32.385
R-25-4	8.53	49.1
R-25-6	12.62	41.109
R-25-7	13.49	43.658
R-50-0	22.31	29.427
R-50-1	18.28	34.787
R-50-4	28.13	38.469
R-50-6	14.21	41.169
R-50-7	12.91	39.646

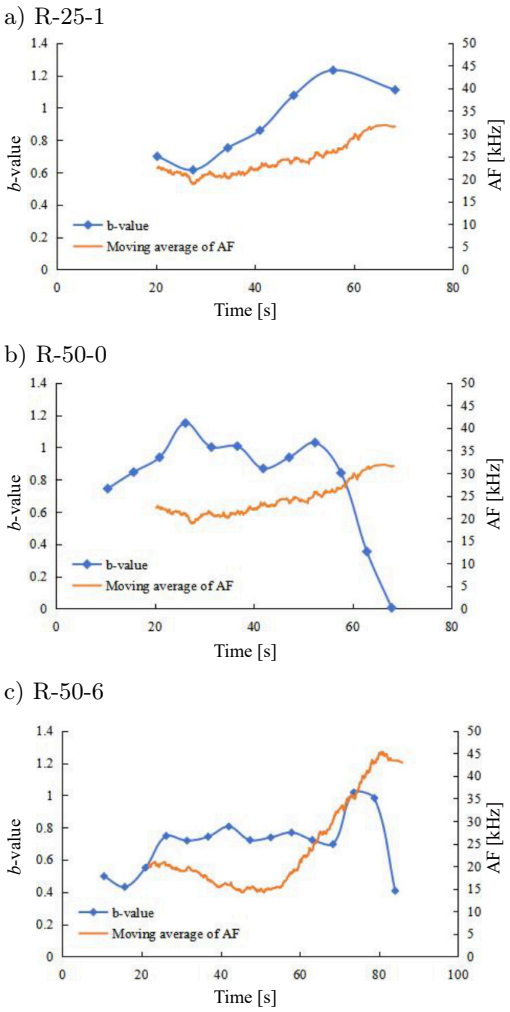

Fig. 8. Relationship between acoustic emission AF moving average of RAC and *b*-value.

R-50-0 test specimen in the 36 s–67 s range. The other is that AF has a low initial value (less than 25 kHz) and decreases continuously. In this scenario, the AE based *b*-value does not show a continuous decrease, indicating that the acoustic emission activity is attenuated, as shown in Fig. 8c, R-50-6 test specimen in the 22 s–48 s range.

5. Conclusions

In this work, the acoustic emission characteristics of polypropylene fiber-reinforced RAC have been researched under uniaxial compression, and the following main conclusions have been drawn:

1) For both R-25-0 and R-50-0 RAC into which no polypropylene fibers are added, the *b*-value exhibits a continuous sharp decrease, indicating that the existence of internal defects in RAC leads to the continuous increase of major event cracking. The initial *b*-value of R-50-0 test specimen is bigger because more initial defects lead to more major event cracking in the initial phase than R-25-0 test specimen. It is found in the re-

search that, for R-25-1, R-25-2, R-50-1, and R-50-2 test specimens into which one kind of fine fiber is added respectively, their b-values do not decrease sharply until the specimens are about to damage. This indicates that with the addition of polypropylene fine fibers, the major event cracking are inhibited. For R-25-4 and R-50-4 test specimens into which only one kind of coarse fiber is added (fiber diameter: 0.9 mm; fiber length: 50 mm), their b-values exhibit a short transition, indicating the intense evolution of microcracks, and then stay stable generally, indicating the stable growth of microcracks, which is mainly due to the bridging effect of coarse fibers.

2) The K-means clustering method has been adopted for two-dimensional clustering analysis of the shear cracking and tensile cracking of the polypropylene fiber-reinforced RAC. The shear cracking is characterized by a high RA value, while the tensile cracking is characterized by a low RA value. The tensile cracking is in the majority in terms of the number of cracking modes. From the perspective of time distribution of cracking, the shear cracking is mainly concentrated in the first half of the elastic-plastic phase; the tensile cracking exists in a large quantity in the compaction, elastic-plastic and post-peak phases; the shear cracking disappears and the tensile cracking is in the majority within 5 s–18 s before the test specimen fails. Therefore, the cracking mechanism of the polypropylene fiber-reinforced RAC under uniaxial compression is dominated by tensile cracking. The SVM has been used to give the hyperplane equations of shear cracking and tensile cracking of polypropylene fiber-reinforced RAC, and the slopes of the linear boundaries of the hyperplane equations are close to 0.

3) The changes in RA and AF moving averages of RAC test specimens with time have been researched. The research shows that, as the RA value decreases, the shear cracking gradually reduces and the tensile cracking gradually increases and dominates. The minimum values of the AF moving averages of most test specimens are negatively correlated with the RAC strength, namely the lower the minimum value of the AF moving average is, the higher the RAC strength will be. There is a certain correlation between the AF value and the AE based b-value. When the AF value increases continuously, the corresponding b-value also increases continuously, indicating an increase in minor event cracking. When the AF value decreases continuously, there are two scenarios. One is that AF has a high initial value (more than 25 kHz) and decreases continuously. In this scenario, the AE based b-value also decreases continuously, indicating an increase in major event cracking; The other is that AF has a low initial value (less than 25 kHz) and decreases continuously. In this scenario, the AE based b-value does not show a continuous decrease, indicating that the acoustic emission activity is attenuated.

Acknowledgments

This study was supported by the Fujian Provincial Natural Science Foundation Projects (grant no. 2022J01930), the authors gratefully acknowledge this support.

References

1. Adamczak-Bugno A., Lipiec S., Vavrus M., Kotes P. (2022a), Non-destructive methods and numerical analysis used for monitoring and analysis of fibre concrete deformations, *Materials*, **15**(20): 7269, doi: 10.3390/ma15207268.
2. Adamczak-Bugno A., Świt G., Krampikowska A., Proverbio E. (2022b), Analysis of the significance of changes in the number and energy parameters of acoustic emission signals on the assessment of the strength of fibre-cement boards, *Materials*, **15**(16): 5757, doi: 10.3390/ma15165757.
3. Aki K. (1965), Maximum likelihood estimate of b in the formula $\log N = a - bM$ and its confidence limits, *Bulletin of the Earthquake Research Institute* (Tokyo), **43**: 237–239.
4. Assaggaf R., Maslehuddin M., Al-Osta M.A., Al-Dulaijan S.U., Ahmad S. (2022), Properties and sustainability of treated crumb rubber concrete, *Journal of Building Engineering*, **51**: 104250, doi: 10.1016/j.jobe.2022.104250.
5. Bai W.F., Shen J.X., Guan J.F., Wang J.Y., Yuan C.Y. (2022), Study on compressive mechanical properties of recycled aggregate concrete with silica fume at different strain rates, *Materials Today Communications*, **31**: 103444, doi: 10.1016/j.mtcomm.2022.103444.
6. Belmokaddem M., Mahi A., Senhadji Y., Pekmezci B.Y. (2020), Mechanical and physical properties and morphology of concrete containing plastic waste as aggregate, *Construction and Building Materials*, **257**: 119559, doi: 10.1016/j.conbuildmat.2020.119559.
7. Chen D.L. *et al.* (2022), Effect of attenuation on amplitude distribution and b value in rock acoustic emission tests, *Geophysical Journal International*, **229**(2): 933–947, doi: 10.1093/gji/ggab480.
8. De Smedt M., Vandecruys E., Vrijdaghs R., Verstrynge E., Vandewalle L. (2022), Acoustic emission-based damage analysis of steel fibre reinforced concrete in uniaxial tension tests, *Construction and Building Materials*, **321**: 126254, doi: 10.1016/j.conbuildmat.2021.126254.
9. Essassi K., Rebiere J.L., El Mahi A., Amine Ben Souf M., Bouguecha A., Haddar M. (2021), Health monitoring of sandwich composites with auxetic core subjected to indentation tests using acoustic emission, *Structural Health Monitoring*, **21**(5): 2264–2275, doi: 10.1177/14759217211053991.
10. Fardoun H., Saliba J., Saiyouri N. (2022), Evolution of acoustic emission activity throughout fine recycled aggregate earth concrete under compressive

tests, *Theoretical and Applied Fracture Mechanics*, **119**: 103365, doi: 10.1016/j.tafmec.2022.103365.

11. GB/T 50081-2019 (2019), *Code for test methods of physical and mechanical properties of concrete* [in Chinese], China Architecture & Building Press, Beijing.
12. Goyal P., Sharma S., Kwatra N. (2021), Evaluation of damage in GFRP repaired steel fiber reinforced concrete beams using acoustic emission technique, *Structural Concrete*, **23**(2): 907–922, doi: 10.1002/suco.202100408.
13. Goyal P., Sharma S., Kwatra N. (2022), Acoustic emission monitoring of steel fiber reinforced beams under simultaneous corrosion and sustained loading, *European Journal of Environmental and Civil Engineering*, **27**(4): 1535–1560, doi: 10.1080/19648189.2022.2087743.
14. Greenhough J., Main I.G. (2008), A Poisson model for earthquake frequency uncertainties in seismic hazard analysis, *Geophysical Research Letters*, **35**(19): L19313, doi: 10.1029/2008GL035353.
15. Guo M.H., Alam S.Y., Bendimerad A.Z., Grondin F., Roziere E., Loukili A. (2017), Fracture process zone characteristics and identification of the micro-fracture phases in recycled concrete, *Engineering Fracture Mechanics*, **181**: 101–115, doi: 10.1016/j.engfracmech.2017.07.004.
16. Gutenberg B., Richter C.F. (1944), Frequency of earthquakes in California, *Bulletin of the Seismological Society of America*, **34**(4): 185–188, doi: 10.1785/BSSA0340040185.
17. Jung D., Yu W.R., Ahn H., Na W.J. (2021), New *b*-value parameter for quantitatively monitoring the structural health of carbon fiber-reinforced composites, *Mechanical Systems and Signal Processing*, **165**: 108328, doi: 10.1016/j.ymssp.2021.108328.
18. Kencanawati N.N., Iizasa S., Shigeishi M. (2013), Fracture process and reliability of concrete made from high grade recycled aggregate using acoustic emission technique under compression, *Materials and Structures*, **46**(9): 1441–1448, doi: 10.1617/s11527-012-9986-z.
19. Kwiatek G., Goebel T.H.W., Dresen G. (2014), Seismic moment tensor and *b* value variations over successive seismic cycles in laboratory stick-slip experiments, *Geophysical Research Letters*, **41**(16): 5838–5846, doi: 10.1002/2014GL060159.
20. Lauff P. *et al.* (2021), Evaluation of the behavior of carbon short fiber reinforced concrete (CSFRC) based on a multi-sensory experimental investigation and a numerical multiscale approach, *Materials*, **14**(22): 7005, doi: 10.3390/ma14227005.
21. Liu X.L., Han M.S., He W., Li X.B., Chen D.L. (2020a), A new *b*-value estimation method in rock acoustic emission testing, *Journal of Geophysical Research-Solid Earth*, **125**(12): e2020JB019658, doi: 10.1029/2020JB019658.
22. Liu X.L., Liu Z., Li X.B., Gong F.Q., Du K. (2020b), Experimental study on the effect of strain rate on rock acoustic emission characteristics, *International Journal of Rock Mechanics and Mining Sciences*, **133**(9): 104420, doi: 10.1016/j.ijrmms.2020.104420.
23. Lockner D.A., Byerlee J.D., Kuksenko V., Ponomarev A., Sidorin A. (1991), Quasi-static fault growth and shear fracture energy in granite, *Nature*, **350**: 39–42, doi: 10.1038/350039a0.
24. MacQueen J. (1967), Some methods for classification and analysis of multivariate observation, [in:] *Proceedings of the Fifth Berkeley Symposium on Mathematical Statistics and Probability*, pp. 281–297.
25. Mandal D.D. *et al.* (2022), Acoustic emission monitoring of progressive damage of reinforced concrete T-beams under four-point bending, *Materials*, **15**(10): 3486, doi: 10.3390/ma15103486.
26. Menna D.W., Genikomsou A.S., Green M.F. (2022), Compressive and cyclic flexural response of double-hooked-end steel fiber reinforced concrete, *Frontiers of Structural and Civil Engineering*, **16**: 1104–1126, doi: 10.1007/s11709-022-0845-x.
27. Prem P.R., Verma M., Ambily P.S. (2018), Sustainable cleaner production of concrete with high volume copper slag, *Journal of Cleaner Production*, **193**: 43–58, doi: 10.1016/j.jclepro.2018.04.245.
28. Prem P.R., Verma M., Ambily P.S. (2021), Damage characterization of reinforced concrete beams under different failure modes using acoustic emission, *Structures*, **30**: 174–187, doi: 10.1016/j.istruc.2021.01.007.
29. Unander T.E. (1993), The effect of attenuation on b-values in acoustic emission measurements – A theoretical investigation, *International Journal of Rock Mechanics and Mining Science & Geomechanics Abstracts*, **30**(7): 947–950, doi: 10.1016/0148-9062(93)90050-N.
30. Utsu T. (1965), A method for determining the value of b in a formula $\log n = a - bm$ showing the magnitude-frequency relation for earthquakes, *Geophysical Bulletin of Hokkaido University*, **13**: 99–103.
31. Vapnik V.N. (1999), An overview of statistical learning theory, [in:] *IEEE Transactions on Neural Networks*, **10**(5): 988–999, doi: 10.1109/72.788640.
32. Watanabe T., Nishibata S., Hashimoto C., Ohtsu M. (2007), Compressive failure in concrete of recycled aggregate by acoustic emission, *Construction and Building Materials*, **21**(3): 470–476, doi: 10.1016/j.conbuildmat.2006.04.002.
33. Weiss J. (1997), The role of attenuation on acoustic emission amplitude distributions and *b*-values, *Bulletin of the Seismological Society of America*, **87**(5): 1362–1367, doi: 10.1785/BSSA0870051362.
34. Xargay H., Ripani M., Folino P., Nunez N., Caggiano A. (2021), Acoustic emission and damage evolution in steel fiber-reinforced concrete beams under cyclic loading, *Construction and Building Materials*, **274**: 121831, doi: 10.1016/j.conbuildmat.2020.121831.
35. Zhang L. (2020), *Study on Damage Evaluation Mechanism of Recycled Concrete in Cold Area* [in Chinese], Inner Mongolia University.